Ground observations of high-latitude Pc3-4 ULF waves

T. A. Howard
School of Physics and Astronomy, University of Birmingham, Edgbaston, UK

F. W. Menk
School of Mathematical and Physical Sciences, University of Newcastle, Callaghan, New South Wales, Australia

Received 3 February 2004; revised 8 December 2004; accepted 13 January 2005; published 9 April 2005.

[1] A detailed study has been undertaken of Pc3-4 waves recorded on the ground with the IMAGE magnetometer array ($56° < \Lambda < 76°$) during January and March 1998. We focus only on daytime events exhibiting high coherence (>0.6) across the entire station array. Most of these had well-defined wave packet appearance in time series records and a clear peak in power spectra. Their occurrence and frequency suggest the waves are generated by the upstream ion-cyclotron resonance mechanism, with no evidence of generation by the Kelvin-Helmholtz instability. For each event the amplitude, phase, coherence, ellipticity, azimuth angle, and degree of polarization across the ground array were examined. The coherence length, azimuthal wave number, and hence the apparent wave propagation velocity were thus determined, with emphasis on the precision and significance of these measurements. It was found that these daytime Pc3-4 pulsations usually have maximum amplitude near the magnetopause projection, meridional coherence lengths of order $1.5-2.0 \times 10^3$ km, and low azimuthal wave numbers during morning hours, averaging around -4.0 (indicating westward propagation). Over 80% of events propagated poleward and westward, with average equivalent ground velocity of 41 km/s N43°W for the H component. About 24–30% of the events are higher harmonics of field line resonances. There is no evidence that the remaining events arise from cavity modes or localized modulated electron precipitation. The observations instead suggest a mechanism involving mode coupling and field-guided propagation. In this model, fast mode waves in the Pc3-4 range entering near the subsolar point propagate earthward and due to the inhomogeneity of the magnetosphere couple to the field-guided Alfvén mode. At certain latitudes, standing oscillations are established at harmonics of the local resonant frequency, while at other latitudes traveling waves convey energy to low altitudes. The expected L dependence of wave power and travel time agree well with observed amplitude and phase profiles.

Citation: Howard, T. A., and F. W. Menk (2005), Ground observations of high-latitude Pc3-4 ULF waves, *J. Geophys. Res.*, *110*, A04205, doi:10.1029/2004JA010417.

1. Introduction

[2] Magnetospheric ULF waves provide a convenient natural probe of the solar-terrestrial interaction and the topology of the magnetosphere [e.g., *Menk et al.*, 1999]. Waves in the Pc3-4 range (~10–100 mHz) are detected in the magnetosphere and on the ground [e.g., *Takahashi et al.*, 1994] and at low and middle latitudes are usually connected with field line resonances (FLRs), i.e., shear Alfvén mode waves oscillating as standing resonant oscillations of geomagnetic field lines [e.g., *Chen and Hasegawa*, 1974; *Menk et al.*, 2000]. For high-latitude ground stations the resonant frequency lies in the Pc5 (~1–10 mHz) range, and ULF waves in this frequency range may be generated by the Kelvin-Helmholtz instability or magnetospheric waveguide modes [*Samson*, 1972; *Samson et al.*, 1991, and references therein]. Pc3-4 waves are also recorded at high latitudes, but the mechanism(s) by which the waves reach these latitudes is not clear.

[3] Previous workers have identified a relationship between the frequency, f, of Pc3-4 ULF waves and the upstream interplanetary magnetic field, B_{IMF} [*Troitskaya et al.*, 1971; *Odera and Stuart*, 1985], generally written as

$$f = 6B_{IMF}. \quad (1)$$

Most recently, the f/B_{IMF} ratio has been given as 4.41 ± 0.25 [*Ponomarenko et al.*, 2002]. It has also been shown that the IMF cone angle, θ_{Bx}, has an influence on Pc3-4 occurrence and energy [e.g., *Bol'shakova and Troitskaya*, 1968; *Wolfe et al.*, 1985], with maximum pulsation power at 0° and

0148-0227/05/2004JA010417$09.00

180°. Relationships between f, B_{IMF} and θ_{Bx} have been obtained theoretically by *Takahashi et al.* [1984],

$$f(\text{mHz}) \sim 7.6 B_{IMF}(\text{nT}) \cos^2 \theta_{Bx}, \quad (2)$$

and empirically by *Le and Russell* [1996],

$$f(\text{mHz}) = (0.72 + 4.67 \cos \theta_{Bx}) B_{IMF}(\text{nT}). \quad (3)$$

The review by *Odera* [1986] provides further details on the relationship between ULF waves and the solar wind.

[4] These apparent dependences suggest that backstreaming reflected ions in the upstream solar wind may enhance incoming ULF fast mode wave energy via ion-cyclotron resonance [*Odera*, 1986, and references therein]. The resultant waves would typically be in the Pc3-4 frequency range and may under appropriate conditions penetrate the magnetosphere and couple to shear Alfvén mode Pc3 FLRs at low latitudes, and Pc4 at midlatitudes [*Yumoto et al.*, 1985]. Their effectiveness in driving Pc3 waves at mid-high latitudes and Pc4 at high latitudes, however, is unclear.

[5] There are several mechanisms by which Pc3-4 ULF waves may propagate to high latitudes. One possibility is that the Pc3-4 are harmonics of fundamental mode Pc5 resonances [e.g., *Fukunishi and Lanzerotti*, 1974; *Tonegawa et al.*, 1984]. Such harmonics would be expected to exhibit the same form of amplitude and phase properties that characterize FLRs [*Kivelson and Southwood*, 1986] and should occur at the same time as the fundamental [*Tonegawa et al.*, 1984]. Another possibility is that Pc3-4 fast mode waves can propagate without mode conversion through the magnetosphere directly to the ionosphere. Such waves are subject to refraction and diffraction on their passage through the magnetosphere [*Moore et al.*, 1987] and may be directed to high latitudes via Fermat's Principle [*Francis et al.*, 1959; *Zhang et al.*, 1993].

[6] Other mechanisms include cavity modes [*Kivelson et al.*, 1984] and the so-called transistor model that invokes beams of precipitating electrons [*Engebretson et al.*, 1991]. The theoretical basis for cavity modes has been established by many workers [e.g., *Kivelson and Southwood*, 1986; *Zhu and Kivelson*, 1989; *Wright*, 1994] but experimental evidence for such modes is sparse [e.g., *Waters et al.*, 2002]. Conversely, many observations have been presented in support of the transistor model [e.g., *Engebretson et al.*, 2000, and references therein]. These ULF waves are characterized by noise-like appearance and low coherence lengths.

[7] This paper attempts to clarify the mechanism(s) by which Pc3-4 ULF waves appear on the ground at high latitudes. To this end, we analyze wave amplitude, coherence, phase, and polarization characteristics for a large number of events recorded with an extensive ground magnetometer array. This work significantly extends a preliminary study reported by *Howard and Menk* [2001], which considered a limited number of isolated events of the type that are readily identified in power spectra. In the present study we use a larger database and relax the selection criteria somewhat. We focus specifically on Pc3-4 ULF waves that exhibit high coherence over large distances and find that while some of these are higher harmonics of FLRs, the majority of the events may arise from field-guided shear Alfvén mode waves produced by mode coupling from incoming fast mode waves.

2. Data and Analysis

2.1. Event Selection

[8] The primary data for this study were obtained from 20 stations of the IMAGE magnetometer array over January and March 1998. The IMAGE array is located in northern Scandinavia and the Arctic [*Lühr et al.*, 1998], spanning $56° < \Lambda < 76°$ (where Λ is the corrected geomagnetic, or CGM latitude), and the magnetometers sample the three geographic components of the geomagnetic field at 0.1 Hz with 0.1 nT resolution. Local time at IMAGE is UT + ~1.5 hours. Data were rotated into geomagnetic coordinates prior to analysis. The spatial extent of the IMAGE array allows wave properties to be examined as a function of latitude and longitude. For this purpose, data were divided into 30 min intervals, each containing 180 sample points. Such an interval containing ULF waves of interest is henceforth referred to as an event.

[9] Event selection involved comparing data from stations near the poleward, equatorward, and central regions of the array. Selection criteria required the following:

[10] 1. A sinusoidal signal lasting at least four cycles in bandpass filtered (typically 5–50 mHz for Pc4 or 15–40 mHz for Pc3) time series for each station. It should be noted that these filters were used for observation only, and the bandpass filter used for analysis was consistently 2–50 mHz.

[11] 2. A clear peak in power at the same frequency at each station.

[12] 3. A peak in coherence (>0.65) at the same frequency as the peak in power across at least three pairs of stations spanning the entire IMAGE array.

[13] 4. A corresponding peak in cross-power across the same three pairs of stations.

[14] For the 2 months we identified 125 events during local daytime satisfying these criteria. Examples of two such events are given in Figure 1. The near-noon event presented in Figure 1b shows typical packet-like appearance associated with discrete relatively band-limited signals that occurred within a distribution of one or more spectral peaks, while the late afternoon event in Figure 1c is more irregular and broadband in appearance. For descriptive purposes these types of events are denoted "packet" and "broad," respectively.

[15] For each event the amplitude, interstation coherence, cross-phase, and polarization were determined using a 180-point FFT with a Hanning window and a frequency resolution of 0.6 mHz. Amplitude values were restored to nT units at a particular frequency and amplitude-latitude profiles produced. Four typical profiles are shown in the top row of Figure 2. All such profiles are plotted against CGM latitude. Each example shown in Figure 2 represents a particular event category; for instance, Figure 2c is an example of an FLR harmonic event. These categories are discussed later. The error bars in the amplitude-latitude profiles represent the magnetometer resolution, ±0.05 nT.

2.2. Coherence and Coherence Length

[16] Coherence, γ, was determined for each event by averaging a series of overlapping subwindows, following

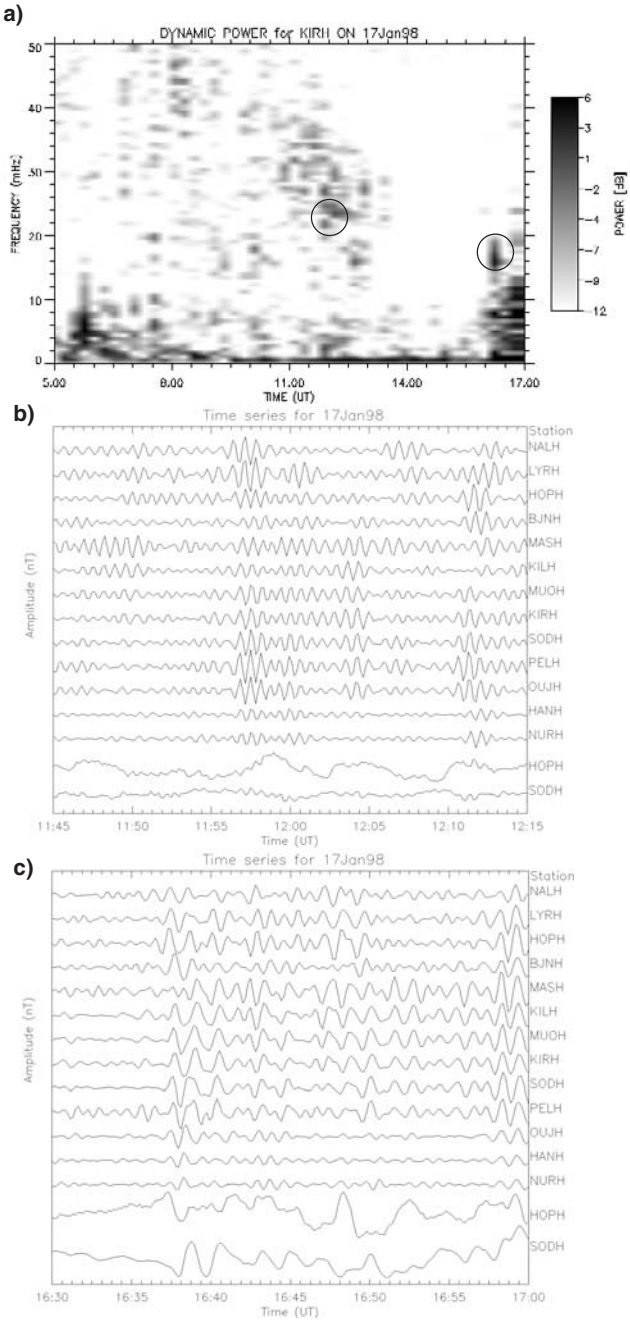

Figure 1. (a) Whole day dynamic power spectrum for 17 January 1998 for the H component of Kiruna (KIR). An example of a "packet" (1145–1215 UT at 20 mHz) and "broad" (1630–1700 UT at 18 mHz) event are indicated by the circles. A bandpass filter from 1 to 50 mHz has been applied. (b) and (c) The equivalent H component time series for each event for a number of IMAGE stations. For the top 10 series, the applied filter was (Figure 1b) 15–30 mHz and (Figure 1c) 10–30 mHz, and the bottom two series are low-pass filtered at 50 mHz.

Fraser [1979]. We used 11, 30-point (5 min) subwindows with 50%-overlap giving a frequency resolution of 3.3 mHz. The number of degrees of freedom, ν, is derived from the number of independent (not overlapping) subwindows (6), multiplied by 2.667 to correct for the effect of the Hanning window [*Jenkins and Watts*, 1968]. Removing the mean, $\nu = 15$. Setting lower (γ_a) and upper (γ_b) coherence limits of 0.00 (representing "noise") and 0.65 ("signal") respectively [*Olson and Szuberla*, 1997; *Howard and Menk*, 2001] and assuming that a Gaussian distribution is formed when the inverse hyperbolic tangent is performed on the coherence of the "noise" [*Jenkins and Watts*, 1968], the confidence percentage for $\eta_{1-\alpha/2}$ can be found using

$$\eta_{1-\alpha/2} = \frac{1}{2}\nu^{1/2}\left[\tanh^{-1}(\gamma_b) - \tanh^{-1}(\gamma_a)\right]. \quad (4)$$

Here, $\eta_{1-\alpha/2}$ is the difference from the mean of each coherence value, normalized into units of standard deviation. For a normal (Gaussian) distribution, centered at the mean, 87% of the values lie within ±1.5 standard deviations from the mean, meaning the probability of finding a random normalized coherence value in this range is 87%. This is the confidence percentage, or α, and $\eta_{0.565} = 1.5$ [*Abramowitz and Stegun*, 1972]. Uncertainties for coherence were derived from $[\tanh^{-1}(\gamma_b) - \tanh^{-1}(\gamma_a)]$, or $\tanh^{-1}(\gamma) \pm 0.39$.

[17] Examples of coherence-latitude profiles (and associated uncertainties) are shown in the second row of Figure 2. Here, Kilpisjärvi (KIL) at 65.8° CGM latitude has been used as the reference station, where by definition $\gamma = 1$. In each case the horizontal dashed line depicts the coherence cutoff for a "signal" at $\gamma = 0.65$.

[18] The coherence length of a signal between any two stations can be determined by assuming that the coherence profile is Gaussian:

$$\gamma = e^{-x^2/X^2}, \quad (5)$$

where x is the interstation distance and X is half the coherence length. The uncertainty range for this coherence length is obtained from the upper and lower limits of γ, represented by the error bars in the coherence profile. Examples of coherence length profiles are shown in the third row of panels in Figure 2. Coherence length was found to depend on interstation distance and so only station pairs that were roughly the same distance (~200 km) apart were used in these profiles. For signals with a high signal-to-noise ratio the coherence length could also be estimated by simply applying a second-order polynomial fit to the coherence-latitude profile and using a cutoff of $\gamma = 0.65$. This method gave similar values to the maximum value in each coherence length-latitude profile.

2.3. Cross-Phase

[19] For each event, information on the variation in phase with latitude and longitude was obtained from both the full 30 min FFT interval [e.g., *Menk et al.*, 2000] and the averaged subwindow technique. To test the accuracy of these measurements and to resolve 2π ambiguities, the phase closure technique was also performed. This involves ensuring that summed interstation phases are consistent when compared across more distant stations.

[20] Examples of phase-latitude profiles are shown in the bottom row of Figure 2, measured relative to the reference station at KIL (65.8°). The convention adopted here is that a positive gradient in a phase-latitude (longitude) profile indicates southward (eastward) propagation.

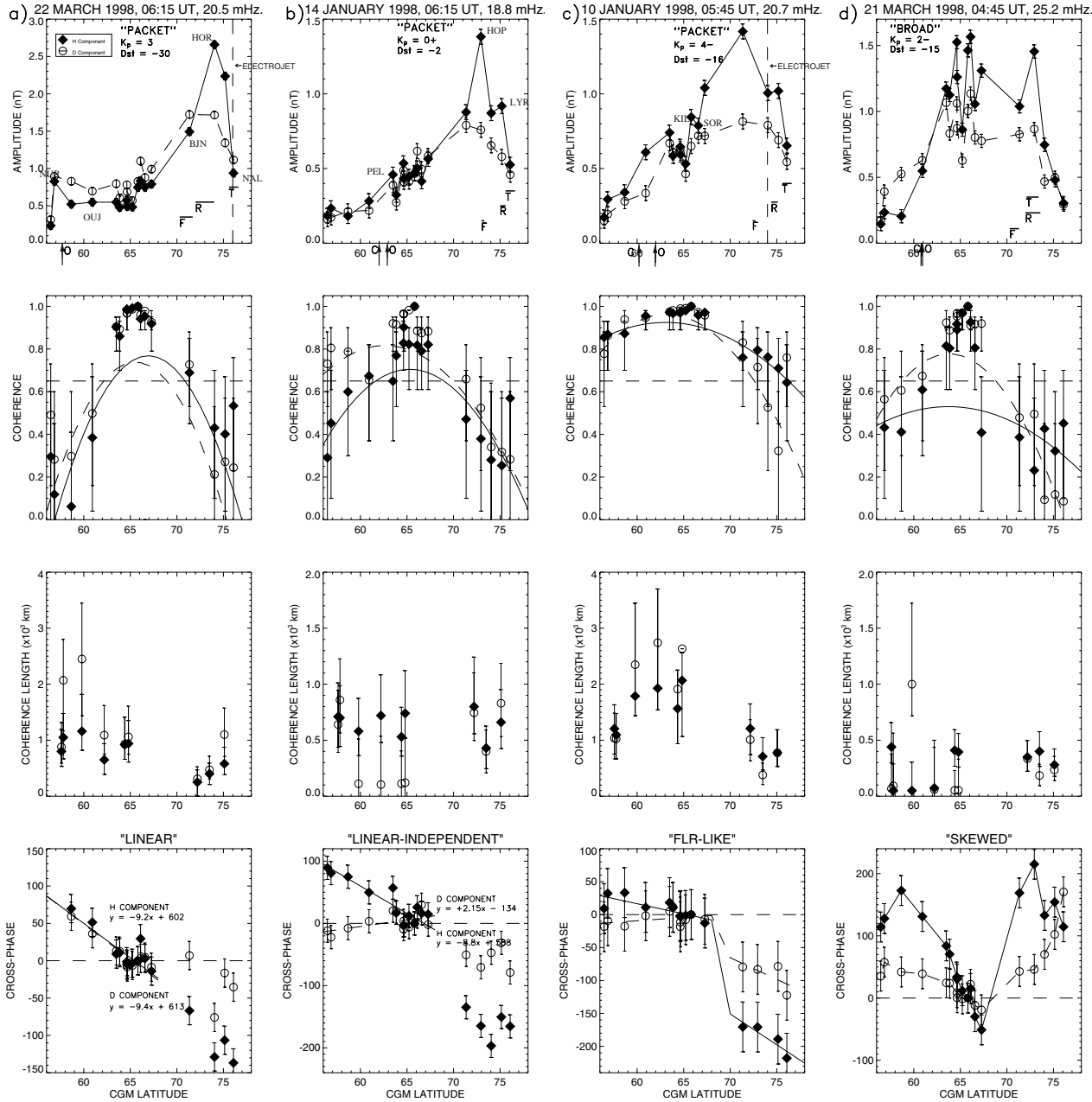

Figure 2. Example profiles of H and D component amplitude (top row), coherence (second), coherence length (third) and phase (bottom), against CGM latitude for four Pc3-4 events: (a) 22 March 1998 at 0615–0645 UT, frequency = 21 mHz, K_p = 3, Dst = −30; (b) 14 January 1998 at 0615–0745 UT, frequency = 19 mHz, K_p = 0+, Dst = −2; (c) 10 January 1998 at 0545–0615 UT, frequency = 21 mHz, K_p = 4−, Dst = −16; (d) 21 March 1998 at 0445–0515 UT, frequency = 25 mHz, K_p = 2−, Dst = −15. Frequency resolution in all cases is 3.3 mHz. Coherence and cross-phase values are relative to a reference station at Kilpisjärvi (KIL). (d) Lines of best fit for the phase profiles are for $\Lambda < 70°$ as shown. The horizontal dashed line in Figure 2b at $\gamma = 0.65$ represents the coherence cutoff. Also shown in the top row are the predicted locations of the magnetopause (shown as horizontal bars) and plasmapause (vertical arrows). Magnetopause locations are labeled according to the models of *Tsyganenko and Stern* [1996] (T), *Rodger* [1998] (R), and *Farrugia et al.* [1989] (F). Plasmapause locations are labeled according to models of *Orr and Webb* [1975] (O) and *Carpenter and Anderson* [1992] (C). Finally, auroral electrojet locations are indicated by the vertical dashed lines. The electrojet is absent from Figures 2b and 2d because it was not defined during the events.

[21] Uncertainty in each cross-phase value is represented by the 87% confidence interval, given the degrees of freedom, ν, the coherence, γ, and the assumption that white noise for cross-phase can be approximated by a Gaussian distribution when the tangent of the phase estimator, $\hat{\varphi}$, is taken. From *Jenkins and Watts* [1968],

$$\tan\hat{\varphi}_{12} \pm \eta_{1-\alpha/2}\sqrt{\sec^4\varphi\left(\frac{1}{\nu}\right)\left(\frac{1}{\gamma^2}-1\right)}, \qquad (6)$$

where φ is the cross-phase measurement. In the cases where the uncertainty due to the sample rate of the IMAGE stations (±2.5 s) was greater than that of the confidence interval, the former was taken.

[22] Also shown in Figure 2 are linear fits for stations spanning the Scandinavian mainland ($\Lambda < 67°$, solid (dashed) for the H (D) component). These provide an estimate of the apparent ground phase speed. Phase-longitude profiles (not shown) were similarly used to estimate the azimuthal wave number, m, taking into account phase-latitude information to correct for any separation in latitude between the measuring stations. The apparent wave ground velocity was then determined using the meridional and azimuthal components of velocity from these cross-phase profiles and then restoring the wavefront.

2.4. Polarization

[23] For each event polarization characteristics were determined from the H and D components at each single station and were based on data from the full 30 min FFT interval. These characteristics were represented by the four Stokes parameters [*Stokes*, 1852]. The following form of the Stokes parameters has been derived from *Fowler et al.* [1967]:

[24] 1. Trace Power: $Tr = S_{hh} + S_{dd}$;

[25] 2. Polarized Power:

$$Pol = \sqrt{(S_{hh} - S_{dd})^2 + 4\left[Re\{S_{hd}\}^2 + Im\{S_{hd}\}^2\right]};$$

[26] 3. Ellipticity: $e = \tan\left[0.5\sin^{-1}\left(\frac{2Im\{S_{hd}\}}{pol}\right)\right]$;

[27] 4. Azimuth: $azim = 0.5\tan^{-1}\left[\frac{2Re\{S_{hd}\}}{(S_{hh}-S_{dd})}\right]$,

where S_{hh} and S_{dd} are the power spectra for the H and D components, respectively, and S_{hd} is the cross-power spectrum. In the present paper, results are shown for only three of the Stokes parameters (excluding Trace Power), with an additional parameter; the degree of polarization, given by $deg = Pol/Tr$. Positive ellipticity corresponds to clockwise rotation or right-handed polarization when looking in the direction of the wave. Positive azimuth angles indicate that the major axis of the polarization ellipse is directed to the north-east quadrant. Examples of the Stokes parameters plotted against latitude are given in Figure 5.

3. General Properties

3.1. Event Occurrence

[28] Figure 3 gives a histogram of event occurrence against time for all 125 daytime events. There is a broad maximum in Pc3-4 occurrence, spanning roughly 0630–1130 UT (0700–1300 LT), or about the subsolar point of the magnetosphere, but with a sharp dip in occurrence prenoon.

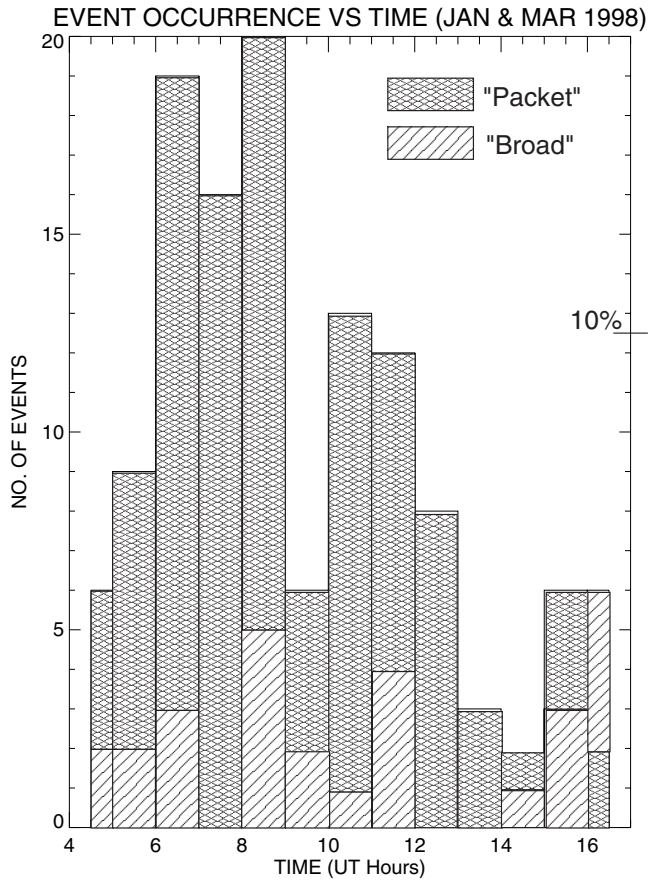

Figure 3. Event occurrence against UT time for the 125 events in January and March, 1998. Events are separated into "packet" and "broad" types. The case labeled "both" is where there is an equal number of packet and broad events.

[29] As stated above, events were classified according to their subjective appearance in power spectra and time series records as of "packet" or "broad" type. "Packet" events accounted for 95, or 76% of the events, while "broad" events were often associated with substorm activity and tended to increase in occurrence toward the dawn-dusk sectors. The time distribution of each type of event is indicated in Figure 3.

[30] More events (74%) occurred in March than in January. This is probably connected with the higher average K_p in March ($\bar{K}_p$ = 2+) than in January ($\bar{K}_p$ = 2−). Many previous workers have reported an increase in high-latitude Pc3-4 occurrence with increasing K_p, and it is well known that geomagnetic activity increases near equinox.

3.2. Relationship With the Interplanetary Magnetic Field

[31] The frequency, f, of each Pc3-4 event was compared with the interplanetary magnetic field strength, B_{IMF}, obtained using the WIND spacecraft MFI magnetometer [*Lepping et al.*, 1995]. Allowances for the time delays between the waves' arrival at WIND and the magnetosphere have been made. A plot of f against B_{IMF} for all 125 events

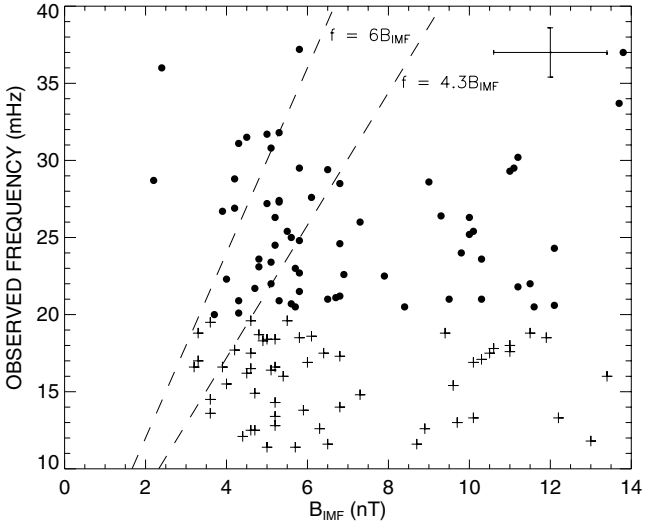

Figure 4. Plot of observed frequency, f, against interplanetary field, B_{IMF}, for the 125 events. Error bars in the top right corner represent the standard deviation in magnetic field measured by the WIND spacecraft and the resolution limits of the observed frequency. Sloping dashed lines correspond to $f = 6B_{IMF}$ and $f = 4.3B_{IMF}$. Those events labeled with a plus symbol were not included in the analysis (see text).

is given in Figure 4. The steepest dashed line indicates $f = 6B_{IMF}$. The average (and one σ uncertainty) of the Pc3 events was $f = (4.3 \pm 2.3)B_{IMF}$, also represented by a dashed line. The large scatter (correlation coefficient, $R^2 < 0.01$) suggests that Pc3-4 frequency does not depend simply on just B_{IMF}. Previous workers [e.g., *Gul'elmi*, 1974; *Green et al.*, 1983] have identified two populations on the f-B_{IMF} relationship, with an apparent difference between events at Pc3 and Pc4 frequencies. Our results, however, do not span a large enough frequency range to make a clear distinction between the two populations; hence we only include results for the Pc3 events, labelling the Pc4 events not used in our analysis as crosses.

[32] Table 1 compares the measured event frequency with the expected frequency calculated using equations given by *Takahashi et al.* [1984] and *Le and Russell* [1996] that include cone angle effects. Approximately 65% of events had frequencies which matched one or the other prediction and 55% matched both simultaneously. Around 75% of the events fell within 2 mHz of the uncertainty range of the predicted frequency in each case. It should be noted that in some cases the cone angles had large uncertainties, resulting in a large range for the frequencies predicted by the models. These results suggest that most of our Pc3 waves are generated in the upstream solar wind, while the generation mechanism for Pc4 is not entirely clear.

4. Case Studies

4.1. Variation in Amplitude With Latitude

[33] Two main types of amplitude-latitude profile were found, one for "packet" events and another for "broad" events. Examples of typical "packet" amplitude-latitude profiles are shown in the top panels of Figures 2a–2c. For most (84 out of 95) of such events amplitude increased with increasing latitude up to a high latitude peak, then decreased beyond that. Similar features were reported by *Bol'shakova and Troitskaya* [1984] and *Engebretson et al.* [1990]. We found the amplitude peak moved equatorward with increasing K_p and decreasing Dst.

[34] The horizontal bars shown in the top panels of Figure 2, labeled "F," "R," or "T," represent three different estimates of the magnetopause latitude. The magnetopause position is usually described in terms of the solar wind ram pressure [*Schield*, 1969] and includes a scaling factor, G. The labels "F" and "R" in Figure 2 relate to $G = (129.4 \pm 2.6)$ and $G = 107.4$ from *Farrugia et al.* [1989] and *Rodger* [1998] and using solar wind data from the WIND spacecraft Solar Wind Experiment (SWE) [*Ogilvie et al.*, 1995]. The labels "T" represent the outermost closed field line latitude for those particular conditions calculated with the Tsyganenko T96 geomagnetic field model [*Tsyganenko and Stern*, 1996].

[35] The amplitude of the "packet" events shown in Figures 2a–2b peaks near the predicted magnetopause region, and for the event in Figure 2c (an FLR event, see below) it peaks just inside the magnetopause. These are general features for many such events. We therefore conclude that these discrete, band-limited, high-coherence Pc3-4 pulsations have maximum amplitude at or just earthward of the magnetopause.

[36] The vertical arrows below the abscissa in Figure 2 represent the location of the plasmapause estimated after *Orr and Webb* [1975] ("O") and *Carpenter and Anderson* [1992] ("C"). In the former case the plasmapause latitude Λ_{pp} depends upon the average K_p for the previous evening (i.e., 2100–0600 LT), and in the latter Λ_{pp} is related to the maximum K_p for the 24 hour period prior to the event. The Pc3-4 amplitudes do not in general change significantly near the expected plasmapause position.

[37] The vertical dashed lines in the top panels of Figure 2 represent the auroral electrojet boundaries, obtained from the IMAGE magnetometer array Web page. Statistically, there is rarely a well defined electrojet system at the times when most of the Pc3-4 events occurred (0600–1200 UT). In some cases, such as on 22 March, the electrojet extends beyond the spatial extent of the IMAGE array, while in others (e.g., 14 January), there is no defined electrojet during the Pc3-4 event. We conclude that the amplitude of Pc3-4 "packet" events is not greatly affected by the presence of the plasmapause or auroral electrojet.

[38] An example amplitude profile for a "broad" event is given in the top panel of Figure 2d. The most prominent

Table 1. Comparison of Event Frequency With Those Determined Using Equations Given By *Takahashi et al.* [1984] and *Le and Russell* [1996][a]

	Fit	≤2 mHz
Takahashi et al. [1984]	84 (67%)	89 (71%)
Le and Russell [1996]	82 (66%)	97 (78%)
Both models	69 (55%)	81 (65%)

[a]The number (and percentage) of events whose frequency fell within the uncertainty range of the predicted frequency is given in the second column, and the number of those within 2 mHz of the predicted frequency is in the third column. The third row represents events that matched both models simultaneously.

feature for these events is the midlatitude peak in amplitude. The distortions in both types of profiles around $\Lambda \sim 65°$ are discussed later. We found that the location of the amplitude peak for the "broad" events was independent of K_p, Dst, and the location of the plasmapause and auroral electrojets.

4.2. Variation in Coherence With Latitude

[39] The second and third rows of panels in Figure 2 show the variation in coherence and coherence length as a function of latitude for the four example events. As discussed earlier, coherence measurements are relative to KIL at 65.8° CGM latitude, and a "signal" cutoff is set at $\gamma = 0.65$. The "packet" events in Figures 2a–2c exhibit high coherence in both H and D components over typically 10° or more in latitude. For the "broad" event in Figure 2d coherence is high over a narrower range in latitude. Coherence lengths are of order 1000 km in latitude for the discrete, band-limited "packet" events, but <500 km for the more noise-like "broad" event. As shown later, these values are typical for such events.

4.3. Variation in Phase With Latitude

[40] We observed four types of phase-latitude behavior for our Pc3-4 events. The bottom row in Figure 2 shows examples of these. For simplicity each type of profile has been assigned a label intended for descriptive purposes only, as follows.

[41] 1. "Linear" profile (e.g., Figure 2a) is where the H and D component phase varies linearly (within about 30°) on latitude except at high latitudes where field lines may be open. We found 10 such events, i.e., 8% of our sample.

[42] 2. "Independent-linear" profile (e.g., Figure 2b) is where the H and D phase profiles are still linear, but the gradient of one component is much greater than for the other. These accounted for 45 (about 36%) of the events and may result from the polarization varying with latitude for events with otherwise "linear" phase profiles.

[43] 3. "FLR-like" events (e.g., Figure 2c) display the characteristic cross-phase signature for an FLR, where there is a phase change of $\sim\pi$ for the H component and somewhat different change in phase for the D component at some latitude. These represented 45 (36%) of the events.

[44] 4. "Skewed" events (e.g., Figure 2d) exhibit a pronounced dip or peak in phase by $\sim\pi$ for the H component at some latitude. This appeared in 25 (20%) of the events.

4.4. Variation in Polarization With Latitude

[45] The polarization Stokes parameters for the four example events are represented by the filled circles (without error bars) in Figure 5. For comparison with the cross-phase profiles the same events are presented here as in Figure 2. We now consider each type of event.

[46] 1. The "linear" event in Figure 5a has fairly consistent azimuth of about −50°, but the ellipticity varies between $e \sim +0.5$ and 0. As shown in Figure 2, the plasmapause and magnetopause were located around latitude 58° and between 70°–76°, respectively, where ellipticity is lowest. Similar features are seen for other "linear" events. The degree of polarization is above 0.5 for most of the example event but approaches unity near the high- and low-latitude edges of the IMAGE array, where the polarized power component of the wave dominates.

[47] 2. The "independent-linear" event in Figure 5b does not seem to show any general trends in ellipticity variations with latitude, but the azimuth and degree of polarization tend to have a greater variance than the "linear" events. This indicates that the shape and orientation of the polarization ellipse is constantly changing. Similar features are seen for many other events of this type.

[48] 3. The "FLR-like" event in Figure 5c exhibits a reversal in the sign of ellipticity between 66° and 71° latitude, where the azimuth angle reaches a maximum, and polarized power peaks around 72°–74° latitude. The sudden change in phase seen for this event in Figure 2 occurred at the same latitude. This event thus displays the features of an FLR [e.g., *Ziesolleck et al.*, 1997] and may be a harmonic of a fundamental Pc5 resonance.

[49] 4. For the "skewed" example in Figure 5d polarized power and ellipticity peak near 65°, where the azimuth angle and degree of polarization also have local peaks. These features are not related to the plasmapause, near 60° latitude, but coincide with the latitude where phase dips to a minimum (Figure 2). Similar properties were observed for many other "skewed" events.

5. Propagation Properties

5.1. Polarization Parameters

[50] Figure 5 includes averages of the three selected Stokes parameters plus the degree of polarization, represented by open circles, for each of the four types of event. Error bars indicate the first standard deviation from the mean. These average plots show the following features:

[51] 1. Polarized power is a maximum at high latitudes near or just equatorward of the magnetopause.

[52] 2. Ellipticity is generally small, typically between 0 and +0.3, indicating nearly linear polarization. However, ellipticity tends to have negative values (left-hand, CCW) at higher latitudes, especially for FLR events.

[53] 3. Azimuth angles are mainly negative, indicating north-west orientation of the polarization ellipse.

[54] 4. The degree of polarization is typically around 0.6 but tends to increase with decreasing latitude.

[55] The polarization properties expected for FLRs were discussed by [*Chen and Hasegawa*, 1974]. Ellipticity should be linear (near-zero) at resonance and polarization should be clockwise (right-hand, positive) for L values just equatorward the resonance location but counterclockwise elsewhere in the morning sector. Moving away from the resonance to lower latitudes, the azimuth angle switches from the northwest to northeast quadrant of the H-D plane (i.e., negative to positive) in the local morning sector.

5.2. Coherence Length

[56] Figure 6a shows meridional (north-south) coherence lengths for the H and D components for all events, plotted against universal time. Filled diamonds represent "packet" events and open squares represent "broad" events. In accord with the examples shown earlier, "packet" events have coherence lengths usually around 1000 km or greater, and these are somewhat larger for the D component than the H. The "broad" events have coherence lengths typically just above the 240 km cutoff imposed by ionospheric spatial integration [*Hughes and Southwood*, 1976].

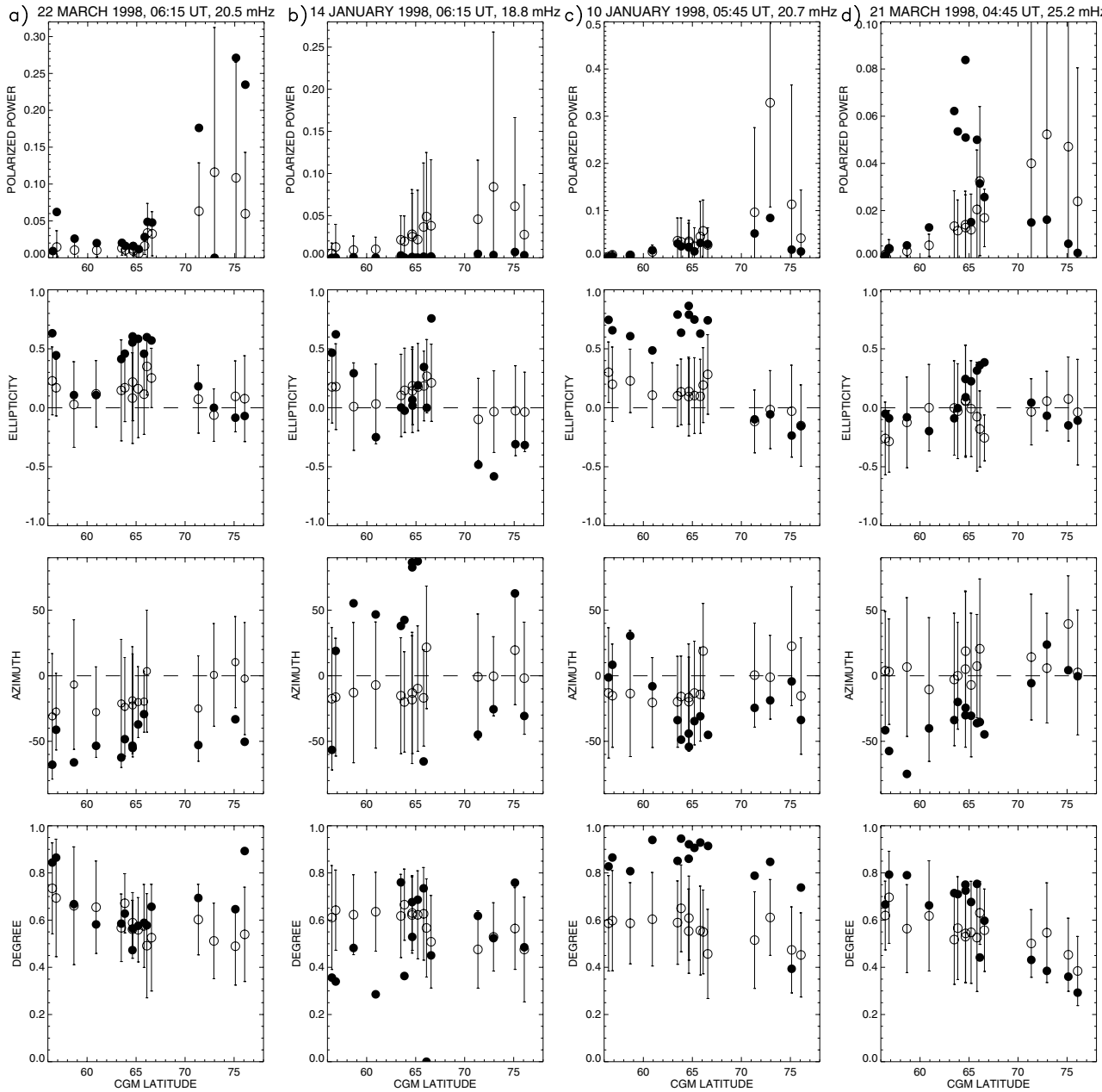

Figure 5. (filled circles) Examples of three of the Stokes parameters (polarized power, ellipticity, azimuth) and the degree of polarization with latitude. The same examples are used here as in Figure 2. Also shown (open circles) are the average Stokes parameter for all events of each type of event along with error bars indicating the first standard deviation from the mean.

[57] These results are summarized in Table 2, which shows that the average coherence lengths are ~1500 (2000) km and 400 (550) km for the "packet" and "broad" event H (D) component, respectively. We found no obvious variation in coherence length for either type of event with time, K_p, or Dst.

5.3. Azimuthal Wave Number (*m* Number)

[58] Azimuthal phase properties were determined for as many events as possible using three or four longitudinally separated stations. Where appropriate, a linear fit was estimated for each resultant phase-longitude profile and an uncertainty, $\delta\varphi$, determined for each fit. Trend lines for which $\delta\varphi \geq 30^\circ$ were deemed unreliable and omitted from the analysis.

[59] Azimuthal wave numbers were obtained from the slopes of these phase-longitude profiles and are summarized in Figure 6b, again separated into "packet" (filled diamond) and "broad" (open square) events. The average *m* numbers were −4.1, $\sigma = 3.2$ (−4.2, $\sigma = 3.9$) for the H (D) component "packet" events and −3.8, $\sigma = 3.0$ (−5.1, $\sigma = 3.3$) for those in the "broad" category, where a negative value indicates westward propagation. Wave numbers were quite variable for events centered on local noon (~1030 UT). Wave numbers for local morning events only are more closely grouped around the mean: H = −4.4, $\sigma = 2.5$, D = −4.8, σ =

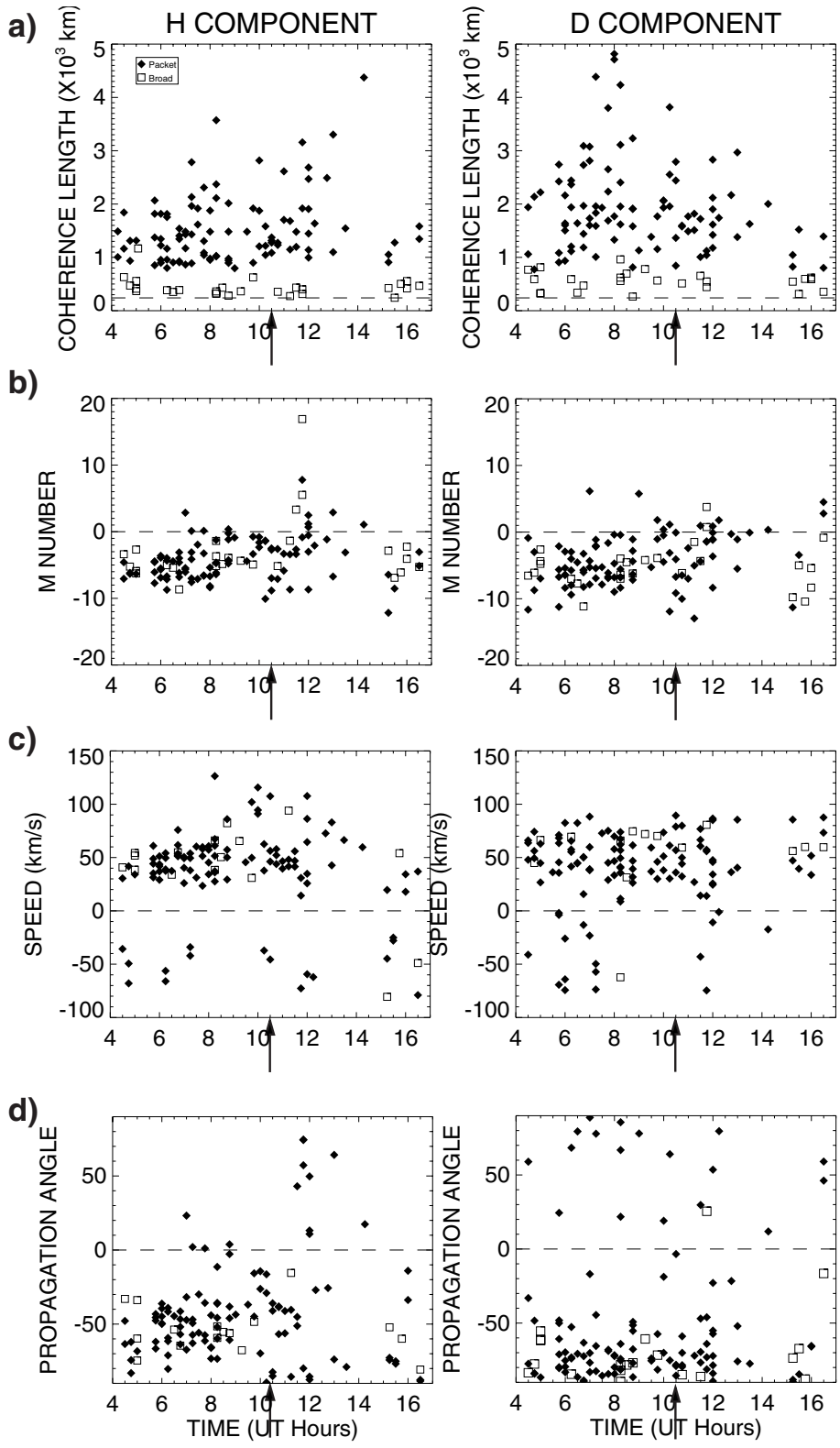

Figure 6. (a) Meridional coherence lengths, (b) azimuthal wave numbers, (c) equivalent ground phase speeds, and (d) propagation angles, for (left) H and (right) D components, when phase uncertainty $\delta\varphi < 30°$. Filled diamonds represent ''packet'' events and open squares denote ''broad'' events. Local noon is indicated by arrows and the horizontal dashed lines in Figure 6a indicate 240 km cutoff due to spatial integration. Positive speed indicates poleward propagation, and propagation angles are positive eastward of the CGM north-south line.

Table 2. Average Coherence Lengths for Discrete Band-Limited "Packet" and More Irregular "Broad" Events for H and D Components[a]

Type	Component	Average Coherence Length ±σ, km
"Packet"	H	$(1.5 \pm 0.7) \times 10^3$
	D	$(2.0 \pm 0.9) \times 10^3$
"Broad"	H	$(4.1 \pm 1.0) \times 10^2$
	D	$(5.5 \pm 1.7) \times 10^2$

[a]Uncertainties represent the standard deviation σ.

3.4, while afternoon values showed greater scatter but were still generally negative.

[60] These results show that azimuthal wave numbers for high-latitude Pc3-4 events are generally low and indicative of westward propagation, except at local noon when the wave numbers are difficult to determine.

5.4. Equivalent Ground Phase Velocity (Speed and Direction)

[61] Figure 6c shows the diurnal distribution in phase speed across the ground, where a positive (negative) sign denotes poleward (equatorward) phase speed. The majority of the H component events (84%) were directed poleward, with an average speed of +52 (σ = 21) km/s. Phase speed did not vary in any obvious way with time, K_p, or Dst.

[62] The wave propagation angles represent the propagation direction of the wavefront, i.e., the angle of the wave ray with respect to the direction of the H component. This was determined by geometrically combining both north-south and east-west components of each event and restoring the wavefront. The angles, plotted against universal time, are shown in Figure 6d. There appears to be a more structured pattern before local noon, while propagation angles especially for the H component are fairly irregular after noon. There is significant scatter in the H (but not D) component near local noon. In total, 82% of the events propagated westward (negative angle), with the average propagation angle being −44°, σ = 32° (−57°, σ = 42°) for the H (D) components.

[63] The average ground phase velocity was hence 41 km/s N43°W for the H component and 2 km/s N57°W for the D component. The low speed of the D component average is due to the roughly even distribution of positive and negative speeds and high variance (σ = 65 km/s) in the D component population. The difference between the average velocities of the two components may result from systematic variation in the average polarization ellipse with latitude.

6. Summary of Observations

[64] In this paper we have considered the propagation of Pc3-4 ULF waves exhibiting high coherence and wave-like properties across the IMAGE ground magnetometer array. From 125 events in 2 months of data, the following features were found:

[65] 1. Event occurrence was higher closer to equinox, when the average K_p was higher.

[66] 2. Narrow-band packet-like events peaked in occurrence prenoon, around 0700–1200 LT.

[67] 3. The observed wave frequency did not depend simply on the magnitude of the upstream IMF but did agree well with predicted frequencies for upstream ion-cyclotron waves when taking into account the solar wind cone angle.

[68] 4. Amplitude-latitude profiles have different appearance for "packet" and "broad" events. Most of the former events peaked in amplitude near or just equatorward of the magnetopause, with the peak latitude moving equatorward with increasing K_p. For "broad" events the maximum amplitude was often reached around 66° CGM latitude and did not depend significantly on K_p.

[69] 5. The amplitude, coherence, or phase of the waves did not change significantly over the expected plasmapause and auroral electrojet latitudes.

[70] 6. For discrete, packet-like waves the phase either varied more or less uniformly with latitude (although the phase gradient may be different for the H and D components) or phase changed by (∼π) in a manner suggestive of FLRs.

[71] 7. For more broadband, noise-like wave events, phase often dipped to a minimum at midlatitudes.

[72] 8. Ellipticity and azimuth of the polarization ellipse varies differently with latitude for different phase profiles. In all cases, polarized power was maximum near the magnetopause latitude. For discrete band-limited events ellipticity was positive (right-handed) at lower latitudes, reducing to zero (linear) near the plasmapause and negative (left-handed) nearer the magnetopause. Azimuth angles generally varied uniformly with latitude, usually being in the NW quadrant. For FLRs ellipticities passed through zero and azimuth angles peaked (i.e., directed to the NE quadrant) at the resonance latitude. For events with a skewed phase-latitude profile (i.e., minimum phase at midlatitudes) ellipticity peaked at near-zero or positive at midlatitude. The degree of polarization was generally ∼0.6 for all events except for the phase skewed events which exhibit low degree of polarization at higher latitudes.

[73] 9. Average coherence length for the discrete "packet" events was $(1.5 \pm 0.7) \times 10^3$ km [$(2.0 \pm 0.9) \times 10^3$] km for the H [D] components. For the more noise-like "broad" events the average coherence length was $(4.1 \pm 1.0) \times 10^2$ km [$(5.5 \pm 1.7) \times 10^2$] km for the H [D] components. D component signals observed on the ground maintain a higher coherence across a larger north-south distance than the H. The azimuthal coherence lengths exceeded the longitudinal extent of the magnetometer array.

[74] 10. The average azimuthal wave number was $m = -4.1 \pm 3.2$ (-4.2 ± 3.9) for the H (D) component. H component m numbers were indeterminate at local noon.

[75] 11. Average ground velocity was 41 km/s N43°W for the H component and 2 km/s (with large variance) N57°W for the D component. If we assume that the observed phase variation is related to a propagation speed then most of the events appear to propagate poleward and westward.

7. Discussion

[76] Here we compare our observational results with predictions from possible generation and propagation mechanisms.

7.1. Generation Mechanisms

7.1.1. Surface Waves (Kelvin-Helmholtz Instability)

[77] It is well known that magnetospheric ULF waves may be generated by the Kelvin-Helmholtz instability

(KHI) [*Chen and Hasegawa*, 1974]. Observational features of such waves have been summarized by *Samson and Rostoker* [1972], *Samson* [1972], and *Olson and Rostoker* [1978]. The waves exhibit near-circular elliptical polarization, with polarization reversal about local noon. Amplitude is maximum around the dawn and dusk flanks and dips around the subsolar point [*Orr*, 1973]. The azimuthal wave number relates to the solar wind speed in the boundary layer, i.e., $m \sim -10$ in the morning sector and $\sim$+10 in the afternoon sector. According to the KHI condition, wave frequency and occurrence should depend on the solar wind plasma density [*Chen and Hasegawa*, 1974].

[78] The polarization profiles in Figure 5 show that all our events exhibited low, near linear ellipticity: $|e| < 0.6$. This does not agree with expectations for a KHI generated wave. We could find no relationship between ellipticity and local time or wave frequency and solar wind number density. Furthermore, Figure 3 shows that peak occurrence for our events was around 0830 UT ($\sim$1000 LT), when occurrence for KHI waves should be approaching a minimum. The azimuthal wave number m for our events was consistently low, averaging around -3 to -4 at all times, much lower than expected for KHI waves.

[79] We therefore conclude that most of the Pc3-4 ULF waves observed in this study were probably not generated by the Kelvin-Helmholtz instability.

7.1.2. Ion Cyclotron Resonance

[80] Magnetospheric ULF waves may also be generated by the upstream ion-cyclotron resonance mechanism, in which case we would expect that (1) the observed wave frequency should depend on B_{IMF}, and more specifically should relate to the model predictions of *Takahashi et al.* [1984] and observations of *Le and Russell* [1996]. (2) Event occurrence should maximize near the subsolar point, typically around 90 minutes before local noon [*Ponomarenko et al.*, 2002]. (3) Waves in the magnetosphere should propagate away from the solar wind entry point.

[81] From our results presented earlier:

[82] 1. Table 1 shows that the frequency for most events matched the *Takahashi et al.* [1984] and *Le and Russell* [1996] predictions, although cone angle uncertainties were large in some cases.

[83] 2. The observed peak in event occurrence around 0800–0900 UT (0930–1030 LT; Figure 3) corresponds well with the expected subsolar wave entry region.

[84] 3. Figures 6c and 6d show that most events propagated across the ground in the north-west direction, i.e., poleward and away from noon for local morning events (the majority of cases). This trend did not continue into the local afternoon. Our measurements of propagation direction may be influenced by other factors that affect wave propagation through the magnetosphere.

[85] These results suggest that many of our Pc3-4 "packet" events were generated in the upstream solar wind by the ion-cyclotron mechanism. It is important to recognize that an incoming wave at a particular (upstream ion-cyclotron) frequency may drive one particular harmonic of a field line resonance at one latitude, and a different harmonic at another. For example, an incoming wave at 15 mHz is the fifth harmonic of a 3 mHz FLR but can also result in observation of third harmonic at a field line of resonance frequency 5 mHz.

7.2. Propagation Mechanisms

7.2.1. Harmonics of FLRs

[86] Pc3-4 pulsations observed on the ground at high latitudes may be higher harmonics of fundamental Pc5 FLRs, possibly excited by higher frequency incoming waves such as those from the ion-cyclotron resonance mechanism [e.g., *Tonegawa et al.*, 1984]. The FLRs should exhibit a local peak in amplitude, rapid π phase change, and a reversal in the sense of rotation of the polarization ellipse across the resonant latitude [e.g., *Samson et al.*, 1971]. Azimuthal wave numbers should be low, typically around 3 [e.g., *Inhester*, 1987]. Taking into account the fact that low-Q resonances show a phase change across larger spatial extents [*Waters et al.*, 1994], we identified 38 Pc3-4 events with clear resonance signatures. However, eight of these had $|m| \geq 8$; removing these from the set yielded average wave numbers (with 1σ uncertainties) of $|m| = 3.0 \pm 2.7$ and 3.1 ± 3.1 for the H and D components.

[87] Our observations thus show that around 25–30% of observed Pc3-4 events were likely higher harmonics of FLRs. This proportion agrees with previous studies at similar latitudes [*Takahashi and McPherron*, 1982; *Ziesolleck et al.*, 1997; *Howard and Menk*, 2001].

7.2.2. Direct Fast Mode Propagation

[88] It is also possible that Pc3-4 waves recorded in polar regions result from fast mode waves generated in the upstream solar wind propagating without mode change through the magnetosphere direct to the ionosphere. Direct propagation of low-frequency (<60 mHz) fast mode ULF waves to high latitudes is prevented by the ion-ion cutoff boundary for the He^+ and O^+ gyroresonances [*Zhang et al.*, 1993], and the waves cannot disperse poleward through the ionosphere as the ionosphere represents a relatively thin layer, almost one-dimensional in comparison with Pc3-4 wavelengths. For direct fast mode propagation, the waves must hence propagate to high latitudes via refraction through the magnetosphere and diffraction around the plasmasphere [*Moore et al.*, 1987; *Zhang et al.*, 1993].

[89] The apparent phase speed across the ground would therefore represent the time of flight of the wavefront through the magnetosphere along a refractive index contour as dictated by Fermat's Principle. An attempt to model a cross-phase-latitude profile based on such a time of flight approach was presented by *Matsuoka et al.* [1997]. They considered a single Pc3 event observed in October 1992 and used an Alfvén speed profile that included a plasmapause density gradient but were more concerned with results at middle and low latitudes.

[90] As discussed above, most of our Pc3-4 events propagated both poleward and away from local noon, corresponding to antisunward propagation away from the equatorial plane. We also found that m number decreased toward local noon, being indefinite at noon (Figure 6b). A similar, but less defined trend is also evident in the the H component propagation angle plot shown in Figure 6d. This could be an indication of decreasing propagation angle as local noon is approached. These observations fit with properties expected for fast mode waves propagating antisunward through the magnetosphere.

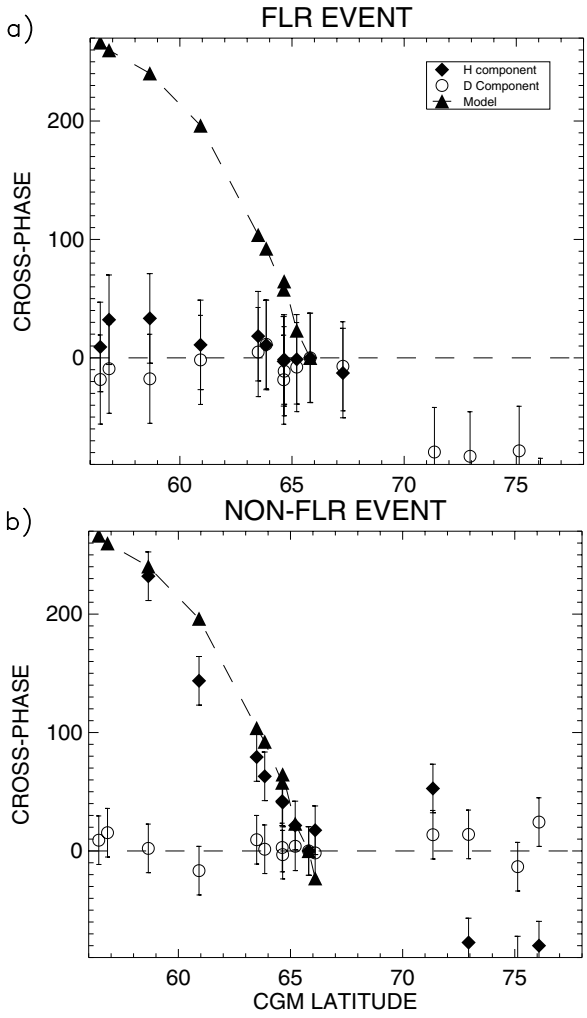

Figure 7. Phase versus latitude profiles for the events on (a) 10 January 1998 at 0545–0615 UT, frequency = 20.9 mHz, and (b) 3 March 1998 at 0745–0815 UT, frequency = 11.4 mHz. In both cases the predicted cross-phase values from *Matsuoka et al.* [1997] along with the H and D components are shown.

[91] We now consider the cross-phase-latitude profile expected for our ground stations for fast mode waves propagating direct through the magnetosphere. For this purpose we extended the phase-latitude profile of *Matsuoka et al.* [1997] to L = 6.5 and using Kilpisjärvi (L = 6.0) as the reference station examined the expected phase-latitude profile for each of our 125 events. Examples of cross-phase-latitude profiles for two representative events are shown in Figure 7. The first event, from 10 January, is an FLR harmonic and the same event shown in Figure 2c. The second event occurred on 3 March and represents a non-FLR event. The modeled cross-phase profile matches observations rather well for the non-FLR event but not at all for the FLR harmonic. Similar matches were found for 49 (52%) of the 95 non-FLR events, although only 16 events were found to have phase values that increased as quickly at low latitudes as the phase values predicted by *Matsuoka et al.* [1997].

[92] A prominent feature in most of the amplitude-latitude profiles is the peak at high latitudes near the magnetopause location, (e.g., Figures 2a and 2b). This is difficult to reconcile with fast mode waves arriving at the ground from the equatorial region unless diffraction around the plasmapause plays a role [e.g., *Moore et al.*, 1987]. However, we could find no obvious relationship between the plasmapause location and that of the amplitude peak.

7.2.3. Cavity Modes

[93] It has long been believed that global cavity modes may play a role in sustaining fast mode magnetospheric ULF waves [e.g., *Kivelson et al.*, 1984]. A suitable cavity may be formed in the outer magnetosphere between the magnetopause and an inner turning point corresponding to a fast mode wave cutoff location, which is frequency dependent [*Harrold and Samson*, 1992; *Waters et al.*, 2000]. The cavity modes thus select compressional wave frequencies that are conveyed to the ground via field lines able to sustain FLRs [e.g., *Waters et al.*, 2002].

[94] We now compare our observations with expected properties if these Pc3-4 waves result from magnetospheric cavity modes.

[95] 1. Amplitude-latitude profiles for cavity modes should exhibit multiple peaks [*Zhu and Kivelson*, 1989; *Waters et al.*, 2002]. We found no evidence of multiple peaks in amplitude at different latitudes; as noted previously our amplitude profiles usually peak near the magnetopause with no clear dominant peaks at lower latitudes.

[96] 2. Cavity resonances should exhibit a number of latitude-dependent sudden changes in phase [e.g., *Zhu and Kivelson*, 1989; *Waters et al.*, 2002]. We did not observe this in our phase-latitude profiles, beyond the local phase dip observed at midlatitudes for the relatively small number of more broadband "skewed" events.

[97] 3. Our observed azimuth and ellipticity properties do not agree with predictions for cavity mode events by *Waters et al.* [2002].

[98] 4. The occurrence and amplitude of cavity mode pulsations should increase with increasing solar wind speed, especially for $V_{SW} > 500$ km/s, as the outer boundary becomes "harder," i.e., a better reflector [*Wright*, 1994; *Mann et al.*, 1999]. A plot of pulsation amplitude against solar wind speed for our events is given in Figure 8. There is no obvious direct relationship between signal amplitude and solar wind speed. In fact, only 29 (23%) of events occurred when solar wind speed exceeded 500 km/s, the peak occurrence being around 400 km/s. Further examination of those 29 events reveals no difference in the amplitude, phase, or polarization properties than for the remainder of the daytime events.

[99] 5. The average azimuthal wave number for all the events was ~ -4. For the subset of events with high solar wind speed the mean m number is -5.1, $\sigma = 3.3$ (6.2, σ = 2.9) for the H (D) component. These values are higher than the mean for all the events, whereas we expect for cavity modes that $m \sim 0$ [*Wright*, 1994].

[100] We therefore conclude that our high latitude Pc3-4 waves are probably not produced by cavity mode resonances.

7.2.4. Transistor Model

[101] The transistor model [*Engebretson et al.*, 1991] requires no wave mode coupling or wave propagation across field lines, rather the modulated precipitation of

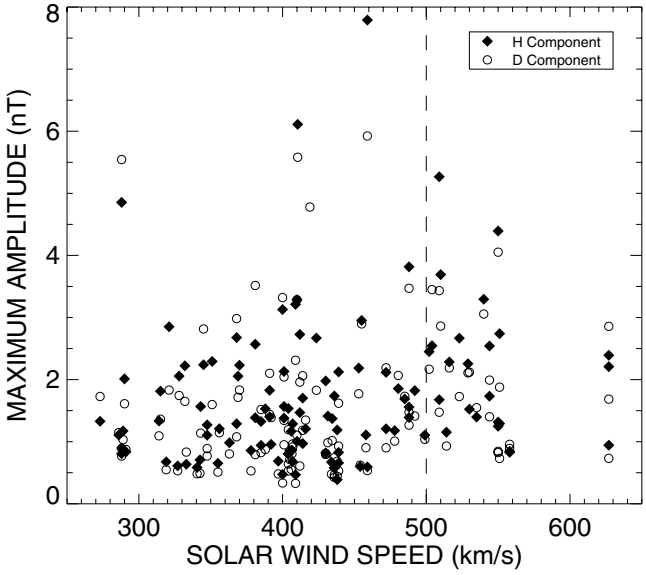

Figure 8. Maximum amplitude against solar wind speed for the 125 events. The cutoff solar wind speed of 500 km/s as suggested by [*Mann et al.*, 1999] is indicated.

electrons in response to pressure fluctuations in the magnetosheath. The latter are attributed to the upstream ion-cyclotron resonance mechanism. The modulated electron beams convey wave information from the outer magnetosphere region containing the parent population of trapped electrons, to the near-cusp ionosphere. The resultant periodic precipitation would modulate the ionospheric conductivity and hence ionospheric currents equatorward of the cusp. Overhead field lines could then be excited by these modulated currents equatorward of the cusp, with the same frequency as the modulated electrons. *Engebretson et al.* [1991] likened this behavior to that of a transistor, where a small base current modulates a larger flow from collector to emitter. While a detailed theoretical treatment of this model remains outstanding [*Olson and Szuberla*, 1997; *Szuberla et al.*, 1998], some predictions can be made based on the physical description of the model. We now attempt to compare the observed Pc3-4 wave properties with these predictions.

[102] The transistor model gives the cusp/cleft as the source region for these waves. The signals should propagate away from the cusp in the ionosphere at near the Alfvén speed, which is of the order of 2000 km/s [e.g., *Waters et al.*, 2000]. The observed propagation direction should vary with local time depending on the ionospheric footprint of the cusp. Wave amplitude should decrease with distance from the cusp, with rapid dissipation due to dispersion in the ionosphere and coupling to overhead magnetic field lines. Also, any factors that affect ionospheric properties, such as the increase in ionospheric conductivity produced by the auroral electrojets or the terminator, would probably affect the signals in some way.

[103] Results from the 125 Pc3-4 events examined in detail in this study reveal no obvious relationship between propagation angle and B_{yIMF} (which is related to the cusp location [*Newell et al.*, 1989]). Amplitude-latitude profiles (e.g., Figures 2a and 2b) show that wave amplitude does not decrease rapidly with distance from the cusp, as amplitudes are still >1 nT at least 30° latitude from the cusp. Only 20 (16%) of our events had velocity directed equatorward for the H-component, and the equivalent propagation speeds are around 2 orders of magnitude lower than the Alfvén speed in the ionosphere. We also found no obvious effects in amplitude-latitude or phase-latitude profiles associated with the location of the auroral electrojets or terminator.

[104] The observational results for our Pc3-4 events therefore do not seem to support the ionospheric transistor model. Note that we only selected and studied events that exhibited high coherence across the entire IMAGE array. Since the transistor model relates to precipitating electron beams in the cusp spatially limited events of that type were probably excluded by our selection criteria.

7.2.5. Field Guided Propagation

[105] We now propose a propagation mechanism to explain how Pc3-4 ULF waves reach the ground at high latitudes, first discussed with relation to FLRs by *Yumoto et al.* [1985] and to traveling waves by *Howard and Menk* [2001]. This involves field-guided traveling waves. It is well known that Pc3-4 fast mode waves penetrate to low latitudes where they can drive FLRs [e.g., *Menk et al.*, 2000]. We now consider incoming fast mode waves that couple to geomagnetic field lines throughout the outer magnetosphere, thus propagating earthward (1) as standing oscillations at harmonics of the local resonant frequency, (2) as quasi-resonances when near a resonant field line, or (3) as weakly coupled travelling waves elsewhere.

[106] We assume the fast mode ULF waves are generated in the upstream solar wind by the ion-cyclotron resonance mechanism and propagate into the magnetosphere in or near the equatorial plane. Mode conversion of the propagating fast/Alfvén mode wave depends on the coupling efficiency, which maximizes at a resonance location [*Inhester*, 1987]. In cases where the fast mode wave is continuous enough to set up a standing wave, we observe a FLR harmonic, while in the remaining (and majority of) cases the mode conversion still occurs, but the resultant shear Alfvén waves propagate to low altitudes as field-guided travelling waves. To the latter we employ the term "quasi-resonances," as they are essentially standing waves which last only a few cycles. Away from the resonance mode coupling also exists but is much weaker. Figure 9 illustrates this model. By assuming an Alfvén speed of 2.0×10^3 km s^{-1}, *Howard and Menk* [2001] showed that the propagation time is longer to a high-latitude station than to a lower-latitude station, resulting in an apparent poleward phase velocity across the ground. *Chi et al.* [2001] also produced propagation delay times based on a more precise magnetospheric model for SSCs and showed that the signal would arrive on the ground at some lower-latitude stations before their higher-latitude neighbors. For example, *Howard* [2003] demonstrated (for a single event) that a wave traveling along a geomagnetic field line mapping to BJN (71.4° CGM) would travel 2.2 R_E further than a wave starting at the same point, traveling in the equatorial plane to a field line mapping to KIL (65.8° CGM), and then along its field line to the ionosphere.

[107] To demonstrate a first attempt at modeling this mechanism, we extend here the approaches of *Chi et al.* [2001] and of *Howard* [2003], who used an example event which occurred on 20 March 1998 at 1045–1115 UT. In

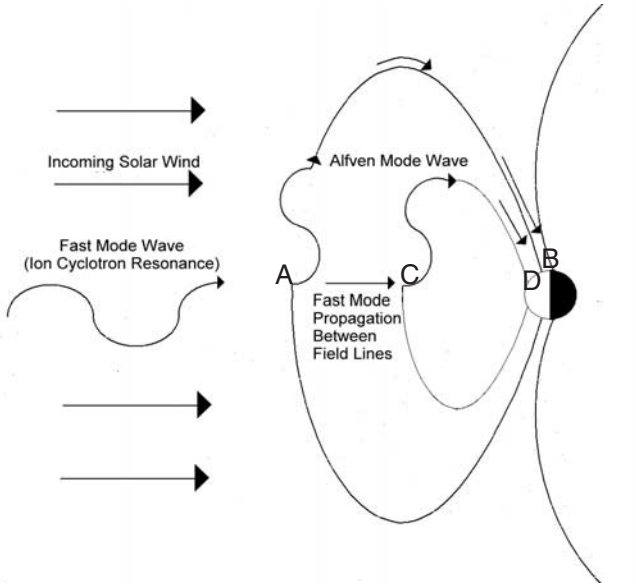

Figure 9. An illustration of the field-guided model. Incoming fast mode waves are converted to Alfvén mode waves upon interaction with geomagnetic field lines, with strongest coupling at those lines favorable to support resonance harmonics. FLR harmonics are established in cases where the fast mode wave is sustained long enough to set up a standing wave, while traveling waves occur when it is not. Fast mode wave propagation continues between resonant field lines. Considering travel times if a wave arrives at point A and propagates along the field line to point B, while the same wave propagates from A to C (an inner field line in the equatorial plane) and then along its field line to D, the distance covered in the latter case is less than that of the former. The wave therefore arrives at D before point B, and propagation on the ground appears to be poleward.

considering how the wave amplitude observed on the ground would vary with latitude, we assumed high efficiency mode conversion at resonant harmonic latitudes and low (and constant) mode conversion efficiency away from the resonance region. An arbitrary value was assigned for the relative increase in amplitude at each resonant field line. There is an uncertainty range in frequency derived from the frequency resolution of ±3.3 mHz, which translates to a latitude uncertainty range using the relationship between resonant frequency and latitude. This latitude range is the full width at half maximum (FWHM) of the peaks, which are 3.5°, 5.0°, and 5.0° latitude for each harmonic, respectively, in the example event. The resultant amplitude-latitude profiles are presented in Figure 10a. The resonance responses shown in the center panel were combined with the standard decay profile for the fast mode component in the top panel to produce the combined response in the bottom panel. Diamonds indicate actual observations for the event on 20 March 1998 discussed by *Howard* [2003]. Note that the highest latitude peak occurs just equatorward of the open-closed field line boundary.

[108] For cross-phase-latitude profile, the T96 [*Tsyganenko and Stern*, 1996] model was used to represent geomagnetic field lines (and B field magnitudes) corresponding to each IMAGE station. Alfvén speed profiles were produced using equatorial density profiles given by *Chappell et al.* [1971], that is,

$$\rho = \rho_0 (r_0/r)^4, \tag{7}$$

where r_0 and ρ_0 are an initial position and density obtained from the Magnetospheric Plasma Analyser aboard the LANL-097A spacecraft [e.g., *Reeves et al.*, 1996, and references therein]. A step-like plasma density to 400 cm^{-3} was also included to represent the plasmasphere. Finally, we simply assumed that the off-equator plasma density is the same as that in the equatorial plane (following *Goldstein et al.* [2001]). This results in a nonconstant Alfvén speed along the field line, as the *B* field magnitude changes. Cross-phase estimates deduced from travel time delays were then combined with the well-known cross-phase signature of an FLR, but with a reduction in the magnitude of the phase change by a factor of three (to represent "quasi resonances"). The modeled cross-phase profile is compared with observations for the example event in Figure 10b.

8. Conclusions

[109] This paper presented results from the analysis of 125 daytime Pc3-4 events recorded across the ground from 56.4° to 76.1° CGM latitude during January and March 1998. The selected events all exhibited high coherence (>0.6) and cross-power across the entire station array. The majority had well-defined wave packet appearance in time series records and a clear peak in power spectra. Occurrence of these events peaked prenoon, near the subsolar point, and their frequency was strongly correlated with that expected for waves generated in the upstream solar wind by the ion-cyclotron mechanism. The remaining events (about 24%) were more irregular and broadband in appearance and were often associated with substorm activity.

[110] For each event we examined the variation with latitude of amplitude, phase, coherence, coherence length, ellipticity, azimuth angle and degree of polarization, and determined the azimuthal wave number and hence the apparent wave propagation velocity across the ground. We assumed "noise" has zero coherence and "signal" has coherence of at least 0.65 and that the coherence profile resembles a Gaussian across an array comprising equally spaced station pairs. One problem with this approach is that since coherence measurements include both "signal" and "noise" contributions, the coherence profiles reflect whichever is dominant. Those with dominant noise measure a coherent signal only across the 240 km region governed by ionospheric spatial integration. The validity of the cross-phase determinations was also expressed through a statistical evaluation. The resultant uncertainties in cross-phase were smaller than those introduced by the timing uncertainty.

[111] We found that packet-like bandlimited Pc3-4 events have maximum amplitude near the magnetopause projection and long coherence lengths: $(1.5 \pm 0.7) \times 10^3$ km for the H component, and $(2.0 \pm 0.9) \times 10^3$ km for the D component. Azimuthal wave numbers were low during morning hours but quite variable at local noon, averaging for local morning events −4.1 ($\sigma = 2.5$) for H and −4.0 ($\sigma = 3.4$) for D. Over

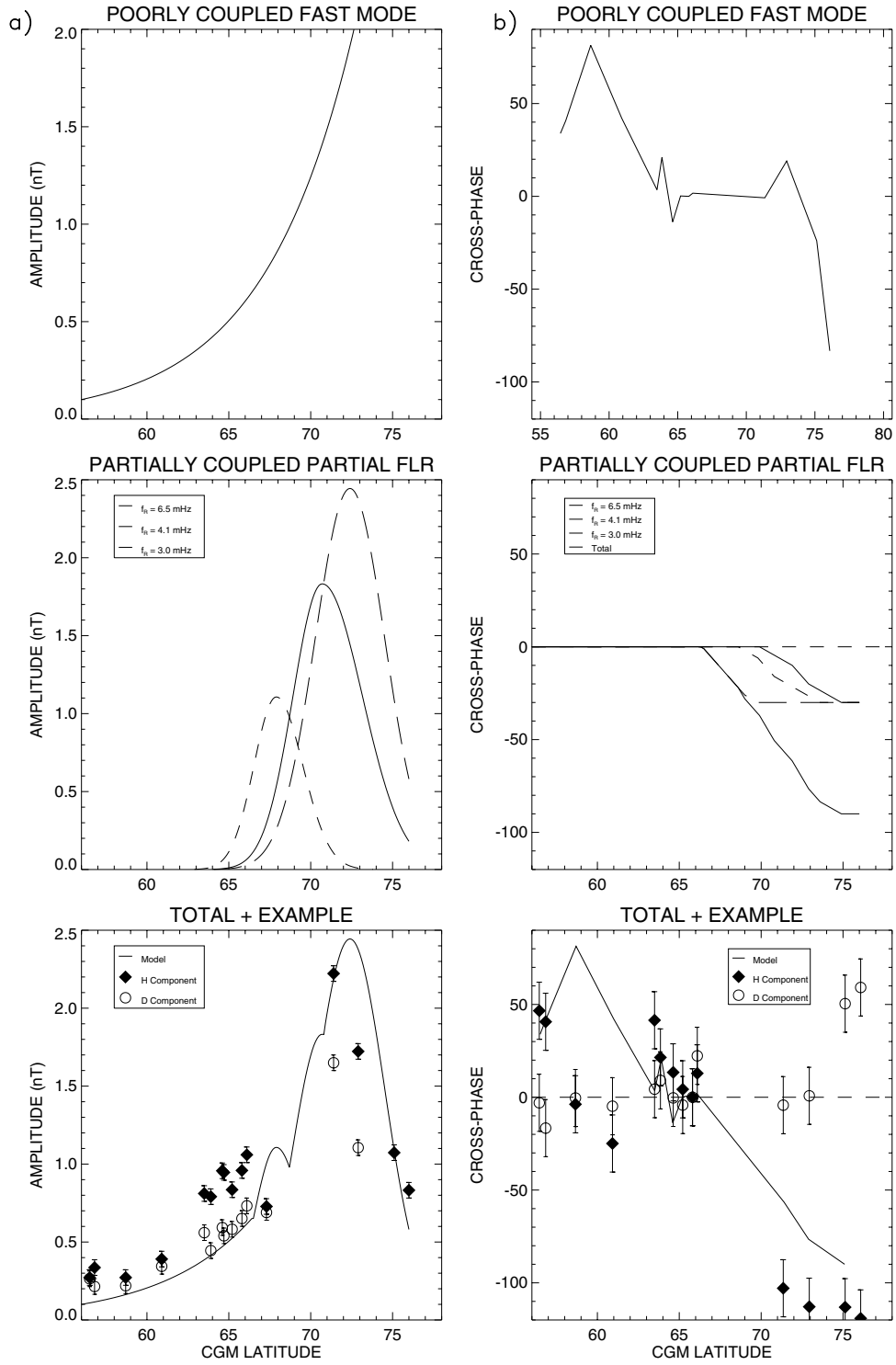

Figure 10. (a) Amplitude and (b) cross-phase profiles estimated by the field-guided model. (top row) The poorly coupled fast mode component; (middle row) partially coupled FLR harmonic component; (bottom row) the combined model along with the H and D results from the example event on 20 March 1998 at 1045 UT.

80% of events propagated poleward and westward, with the average equivalent ground velocity being 41 km/s N43°W for the H component.

[112] The phase and polarization profiles show that about 24–30% of the packet-like daytime Pc3-4 events are higher harmonics of field line resonances. There is no evidence that these are generated by a Kelvin-Helmholtz instability, and it seems most likely that incoming fast mode waves at a frequency determined by the upstream ion-cyclotron resonance couple to FLRs at a harmonic of the eigenfrequency.

[113] For the remaining, non-FLR events we considered three possible propagation mechanisms:

[114] 1. The observed amplitude, phase, and polarization properties do not agree with what we would expect if the waves resulted from cavity modes in the outer magnetosphere.

[115] 2. Fast mode waves may propagate without mode change through the magnetosphere direct to the ionosphere along paths determined by the refractive index and diffraction effects around the plasmapause. This can explain the observed poleward propagation across the ground for about half of the non-FLR events but is difficult to reconcile with the peak in amplitude at high latitudes.

[116] 3. The transistor model of *Engebretson et al.* [1991] considers electron precipitation in the cusp modulated by Pc3-4 waves in the outer magnetosphere. We could not explain the observed amplitude, phase, or polarization properties of our high coherence length, bandlimited Pc3-4 events with this mechanism. However, our selection criteria excluded more localized signals discussed by, e.g., *Engebretson et al.* [1990] and *Olson and Szuberla* [1997]. While our high coherence length propagating Pc3-4 waves may be a source of similar signals at low latitudes [e.g., *Takahashi et al.*, 1994], they may provide only a minor contribution to the overall Pc3-4 spectrum at high latitudes. For instance, if we relax the selection criteria to include events with high coherence and common peaks in cross-power across only half instead of the entire IMAGE array (i.e., either the high- or low-latitude part), 1360 "events" are identified. This suggests that our packet-like events may contribute less than 10% to the total Pc3-4 ULF wave power observed locally. Furthermore, in selecting high coherence events we may be excluding signals occurring on open field lines, e.g., at high K_p.

[117] Our observations of daytime packet-type Pc3-4 waves suggest a mechanism involving mode coupling and field-guided propagation. Following *Howard and Menk* [2001], we propose that fast mode waves in the Pc3-4 range enter the magnetosphere near the subsolar point and propagate earthward initially in or near the equatorial plane. Owing to the inhomogeneity of the magnetosphere the waves couple to the field-guided Alfvén mode. At latitudes where frequencies match standing oscillations, FLR harmonics are established at the local resonant frequency, while at other latitudes traveling field-guided waves convey energy to low altitudes. The observed amplitude-latitude and phase-latitude profiles agree well with simple model predictions based on the wave attenuation and differential travel time in the equatorial plane and along field lines.

[118] The more irregular and broadband events exhibit quite different properties to the packet-like events summarized above. The former reach peak amplitude at midlatitudes, exhibit a strong dip in phase at the same latitude, and have much lower coherence lengths, of order 400–500 km. Their generation and propagation mechanisms are not clear.

[119] Finally, we note that many amplitude profiles show a distortion around $64.6° \leq \Lambda \leq 66.1°$. This anomaly always occurred at the same stations, independent of the location of the plasmapause, auroral electrojet, K_p, and Dst. A similar feature appears in the IMAGE results presented by *Mathie and Mann* [2000] for Pc5 frequencies. This feature is most likely due to ground induction effects such as those detected near Masi ($\Lambda = 66.1°$, $\Phi = 106.9°$) [*Viljanen et al.*, 1995]. We have been careful not to let such effects influence our phase or velocity results.

[120] **Acknowledgments.** We thank P. V. Ponomarenko and C. L. Waters at the School of Mathematical and Physical Sciences, University of Newcastle for helpful discussions. This work was supported by the Australian Research Council, the University of Newcastle, and the Cooperative Research Centre for Satellite Systems through the Commonwealth of Australia CRC Program. IMAGE data were obtained by request to the administrators of the network at the IMAGE Web site (http://www.geo.fmi.fi/image/), and we thank the Finnish Meteorological Institute and the institutes who maintain the array. Data from the MFI and SWE aboard WIND were made available courtesy of R. P. Lepping and K. W. Ogilvie at Goddard Space Flight Center and CDAWeb (http://cdaweb.gsfc.nasa.gov/).

[121] Lou-Chuang Lee thanks Nagendra Singh and another reviewer for their assistance in evaluating this paper.

References

Abramowitz, M., and I. A. Stegun (Eds.) (1972), *Handbook of Mathematical Functions*, Dover, Mineola, N. Y.

Bol'shakova, O. V., and V. A. Troitskaya (1968), Relation of the IMF direction to the system of stable oscillations, *Dokl. Akad. SSSR*, *180*, 343.

Bol'shakova, O. V., and V. A. Troitskaya (1984), The relation of the high latitude maximum of Pc3 intensity to the dayside cusp, *Geomagn. Aeron.*, *24*, 633–635.

Carpenter, D. L., and B. J. Anderson (1992), An ISEE/whistler model of equatorial electron density in the magnetosphere, *J. Geophys. Res.*, *97*, 1097–1108.

Chappell, C. R., K. K. Harris, and G. W. Sharp (1971), The dayside of the plasmasphere, *J. Geophys. Res.*, *76*, 7632–7647.

Chen, L., and A. Hasegawa (1974), A theory of long-period magnetic pulsations: 1. Steady state excitation of field line resonance, *J. Geophys. Res.*, *79*, 1024–1032.

Chi, P. J., et al. (2001), Propagation of preliminary reverse impulse of sudden commencements to low latitudes, *J. Geophys. Res.*, *106*, 18,857–18,864.

Engebretson, M. J., B. J. Anderson, L. J. Cahill Jr., R. L. Arnoldy, T. J. Rosenberg, D. L. Carpenter, W. B. Gail, and R. H. Eather (1990), Ionospheric signatures of cusp latitude Pc3 pulsations, *J. Geophys. Res.*, *95*, 2447–2456.

Engebretson, M. J., L. J. Cahill Jr., R. L. Arnoldy, B. J. Anderson, T. J. Rosenberg, D. L. Carpenter, U. S. Inan, and R. H. Eather (1991), The role of the ionosphere in coupling upstream ULF wave power into the dayside magnetosphere, *J. Geophys. Res.*, *96*, 1527–1542.

Engebretson, M. J., R. K. Cobian, and J. L. Posch (2000), A conjugate study of Pc3-4 pulsations at cusp latitudes: Is there a clock angle effect?, *J. Geophys. Res.*, *105*, 15,965–15,980.

Farrugia, C. J., M. P. Freeman, S. W. H. Cowley, and D. J. Southwood (1989), Pressure-driven magnetopause motions and attendant response on the ground, *Planet. Space Sci.*, *37*, 589–607.

Fowler, R. A., B. J. Kotick, and R. D. Elliot (1967), Polarization analysis of natural and artificially induced geomagnetic pulsations, *J. Geophys. Res.*, *72*, 2871–2883.

Francis, W. E., M. I. Green, and A. J. Dessler (1959), Hydromagnetic propagation of sudden commencements of magnetic storms, *J. Geophys. Res.*, *64*, 1643–1645.

Fraser, B. J. (1979), The use of multistation networks in geomagnetic pulsation studies, *Ann. Telecommun.*, *35*, 1/17.

Fukunishi, H., and L. J. Lanzerotti (1974), ULF pulsation evidence of the plasmapause: 1. Spectral studies of Pc3 and Pc4 pulsations near L = 4, *J. Geophys. Res.*, *79*, 142–158.

Goldstein, J., R. E. Denton, M. K. Hudson, E. G. Miftakhava, S. L. Young, J. D. Menietti, and D. L. Gallagher (2001), Latitudinal density dependence of magnetic field lines inferred from Polar plasma wave data, *J. Geophys. Res.*, *106*, 6195–6201.

Green, C. A., T. J. Odera, and W. F. Stuart (1983), The relationship between the strength of the IMF and the frequency of magnetic pulsations on the ground and in the solar wind, *Planet. Space Sci.*, *31*, 559–567.

Gul'elmi, A. V. (1974), Diagnostics of the magnetosphere and interplanetary medium by means of pulsations, *Space Sci. Rev.*, *16*, 331–345.

Harrold, B. G., and J. J. Samson (1992), Standing ULF modes in the magnetosphere: A theory, *Geophys. Res. Lett.*, *19*, 1811–1814.

Howard, T. A. (2003), The generation and propagation of Pc3-4 ULF waves at high latitudes, Ph.D. thesis, Univ. of Newcastle, Callaghan, Australia.

Howard, T. A., and F. W. Menk (2001), Propagation of 10–50 mHz ULF waves with high spatial coherence at high latitudes, *Geophys. Res. Lett.*, *28*, 231–234.

Hughes, W. J., and D. J. Southwood (1976), An illustration of modification of geomagnetic pulsation structure by the ionosphere, *J. Geophys. Res.*, *81*, 3241–3247.

Inhester, R. (1987), Numerical modelling of hydromagnetic wave coupling in the magnetosphere, *J. Geophys. Res.*, *92*, 4751–4756.

Jenkins, G. M., and D. G. Watts (1968), *Spectral Analysis and Its Applications*, Holden Day, Boca Raton, Fla.

Kivelson, M. G., and D. J. Southwood (1986), Coupling of global magnetospheric mhd eigenmodes to field line resonances, *J. Geophys. Res.*, *91*, 4345–4351.

Kivelson, M. G., J. Etcheto, and J. G. Trotignon (1984), Global compression oscillations of the terrestrial magnetosphere: The evidence and a model, *J. Geophys. Res.*, *89*, 9851–9856.

Le, G., and C. T. Russell (1996), Solar wind control of upstream wave frequency, *J. Geophys. Res.*, *101*, 2571–2575.

Lepping, R. P., et al. (1995), The WIND magnetic field investigation, *Space Sci. Rev.*, *71*, 207–229.

Lühr, H., A. Aylward, S. C. Buchert, A. Pajunpää, T. Holmboe, and S. M. Zalewski (1998), Westward moving dynamic substorm features observed with the IMAGE magnetometer network and other ground-based instruments, *Ann. Geophys.*, *16*, 425–440.

Mann, I. R., A. N. Wright, K. J. Mills, and V. M. Nakariakov (1999), Excitation of magnetospheric waveguide modes by magnetosheath flows, *J. Geophys. Res.*, *104*, 333–353.

Mathie, R. A., and I. R. Mann (2000), Observations of Pc5 field line resonance azimuthal phase speeds: A diagnostic of their excitation mechanism, *J. Geophys. Res.*, *105*, 10,713–10,728.

Matsuoka, H., K. Takahashi, S. Kokubun, K. Yomoto, T. Yamamoto, S. I. Soloyev, and E. F. Vershinin (1997), Phase and amplitude structure of Pc3 magnetic pulsations as determined from multipoint observations, *J. Geophys. Res.*, *102*, 2391–2403.

Menk, F. W., D. Orr, M. A. Clilverd, A. J. Smith, C. L. Waters, D. K. Milling, and B. J. Fraser (1999), Monitoring spatial and temporal variations in the dayside plasmasphere using geomagnetic field line resonances, *J. Geophys. Res.*, *104*, 19,955–19,970.

Menk, F. W., C. L. Waters, and B. J. Fraser (2000), Field line resonances and waveguide modes at low latitudes: 1. Observations, *J. Geophys. Res.*, *105*, 7747–7762.

Moore, T. E., D. L. Gallagher, J. L. Horwitz, and R. H. Comfort (1987), MHD wave breaking in the outer plasmasphere, *Geophys. Res. Lett.*, *14*, 1007–1010.

Newell, P. T., C.-I. Meng, D. G. Sibeck, and R. Lepping (1989), Some low-altitude cusp dependences on the interplanetary magnetic field, *J. Geophys. Res.*, *94*, 8921–8927.

Odera, T. J. (1986), Solar wind controlled pulsations, *Rev. Geophys.*, *24*, 55–74.

Odera, T. J., and W. F. Stuart (1985), The relationship between the IMF magnitude and the frequency of Pc3, 4 pulsations on the ground: Simultaneous events, *Planet. Space Sci.*, *33*, 387–393.

Ogilvie, K. W., et al. (1995), SWE: A comprehensive plasma instrument for the Wind spacecraft, *Space Sci. Rev.*, *71*, 55–77.

Olson, J. V., and G. Rostoker (1978), Longitudinal phase variation of Pc4-5 micropulsations, *J. Geophys. Res.*, *83*, 2481.

Olson, J. V., and C. A. L. Szuberla (1997), A study of Pc3 at cusp latitudes, *J. Geophys. Res.*, *102*, 11,375–11,384.

Orr, D. (1973), Magnetic pulsations within the magnetosphere: A review, *J. Atmos. Terr. Phys.*, *35*, 1–50.

Orr, D., and D. C. Webb (1975), Statistical studies of geomagnetic pulsations with periods between 10 and 70 sec and their relationship to the plasmapause region, *Planet Space Sci.*, *23*, 1169–1178.

Ponomarenko, P. V., B. J. Fraser, F. W. Menk, S. T. Ables, and R. J. Morris (2002), Cusp-latitude Pc3 spectra: Band limited and power law components, *Ann. Geophys.*, *20*, 1539–1551.

Reeves, G. D., M. G. Henderson, P. S. McLachlan, R. D. Belian, R. H. W. Freidel, and A. Korth (1996), Radial propagation of substorm injections, in *Proceedings of Third International Conference on Substorms*, *ESA SPP-389*, edited by E. J. Rolph and B. Kaldeich, Eur. Space Agency, Noordwijk, Netherlands.

Rodger, A. S. (1998), Ionospheric signatures of magnetospheric processes, in *Polar Cap Boundary Phenomena*, edited by J. Moen, A. Egeland, and M. Lockwood, p. 115, Springer, New York.

Samson, J. C. (1972), Three-dimensional polarization characteristics of high latitude Pc5 geomagnetic pulsations, *J. Geophys. Res.*, *77*, 6145–6160.

Samson, J. C., and G. Rostoker (1972), Latitude-dependent characteristics of high-latitude Pc4 and Pc5 micropulsations, *J. Geophys. Res.*, *77*, 6133–6144.

Samson, J. C., J. A. Jacobs, and G. Rostoker (1971), Latitude-dependent characteristics of long-period geomagnetic micropulsations, *J. Geophys. Res.*, *76*, 3675–3683.

Samson, J. C., R. A. Greenwald, J. M. Ruohoniemi, T. A. Hughes, and D. D. Wallis (1991), Magnetometer and radar observations of magnetohydrodynamic cavity modes in the Earth's magnetosphere, *Can. J. Phys.*, *69*, 929–937.

Schield, M. A. (1969), Pressure balance between solar wind and magnetosphere, *J. Geophys. Res.*, *74*, 1275–1286.

Stokes, G. G. (1852), *Trans. Cambridge Phil. Soc.*, *9*, 302.

Szuberla, C. A. L., J. V. Olson, M. J. Engebretson, B. J. Fraser, and S. T. Ables (1998), Interstation Pc3 occurrence at cusp latitudes, *Geophys. Res. Lett.*, *25*, 2381–2384.

Takahashi, K., and R. L. McPherron (1982), Harmonic structure of Pc3-4 pulsations, *J. Geophys. Res.*, *87*, 1504–1516.

Takahashi, K., R. L. McPherron, and T. Terasawa (1984), Dependence of the spectrum of Pc3-4 pulsations on the interplanetary magnetic field, *J. Geophys. Res.*, *89*, 2770–2780.

Takahashi, K., B. J. Anderson, T. Yamamoto, and N. Sato (1994), Propagation of compressional Pc3 pulsations from space to the ground: A case study using multipoint measurements, in *Solar Wind Sources of Magnetospheric Ultra-Low Frequency Waves*, *Geophys. Monogr. Ser.*, vol. 81, edited by M. J. Engebretson, K. Takahashi, and M. Scholer, p. 355, AGU, Washington, D. C.

Tonegawa, Y., H. Fukunishi, T. Hirasawa, R. L. McPherron, T. Sakurai, and Y. Kato (1984), Spectral characteristics of Pc3 and Pc4/5 magnetic pulsation bands observed near L = 6, *J. Geophys. Res.*, *89*, 9720–9730.

Troitskaya, V. A., T. A. Plyasova-Bakounina, and A. V. Gul'elmi (1971), Relationship between Pc2-4 pulsations and the interplanetary field, *Dokl. Akad. Nauk. SSSR*, *197*, 1313.

Tsyganenko, N. A., and D. P. Stern (1996), Modelling the global magnetic field of the large-scale Birkeland current systems, *J. Geophys. Res.*, *101*, 27,187–27,198.

Viljanen, A., K. Kauristie, and K. Pajunpää (1995), On induction effects as EISCAT and IMAGE magnetometer stations, *Geophys. J. Int.*, *121*, 893–906.

Waters, C. L., F. W. Menk, and B. J. Fraser (1994), Low latitude geomagnetic field line resonance: Experiment and modelling, *J. Geophys. Res.*, *99*, 17,547–17,558.

Waters, C. L., B. G. Harrold, F. W. Menk, J. C. Samson, and B. J. Fraser (2000), ULF waveguide mode waves at low latitudes: 2. A model, *J. Geophys. Res.*, *105*, 7763–7774.

Waters, C. L., K. Takahashi, D.-H. Lee, and B. J. Anderson (2002), Detection of ultralow-frequency cavity modes using spacecraft data, *J. Geophys. Res.*, *107*(A10), 1284, doi:10.1029/2001JA000224.

Wolfe, A., A. Meloni, L. J. Lanzerotti, C. G. MacLennan, J. Bamber, and D. Venkatesan (1985), Dependence of hydromagnetic energy spectra near L = 2 and L = 3 on upstream solar wind parameters, *J. Geophys. Res.*, *90*, 5117–5131.

Wright, A. N. (1994), Dispersion and wave coupling in inhomogeneous mhd waveguides, *J. Geophys. Res.*, *99*, 159–167.

Yumoto, K., T. Saito, S.-I. Akasofu, B. T. Tsurutani, and E. J. Smith (1985), Propagation mechanism of daytime Pc3-4 pulsations observed at synchronous orbit and multiple ground-based stations, *J. Geophys. Res.*, *90*, 6439–6450.

Zhang, X., R. H. Comfort, Z. E. Musielak, T. E. Moore, D. L. Gallagher, and J. L. Green (1993), Propagation characteristics of Pc3 compressional waves generated at the dayside magnetopause, *J. Geophys. Res.*, *98*, 15,403–15,410.

Zhu, X., and M. G. Kivelson (1989), Global mode ULF pulsations in a magnetosphere with a nonmonotonic Alfvén velocity profile, *J. Geophys. Res.*, *94*, 1479–1485.

Ziesolleck, C. W. S., D. R. McDiarmid, and Q. Feng (1997), A comparison between the Pc3-4 pulsations observed by GOES 7 and the CANOPUS magnetometer array, *J. Geophys. Res.*, *102*, 4893–4909.

T. A. Howard, School of Physics and Astronomy, University of Birmingham, Edgbaston, B15 2TT, UK. (tim@star.sr.bham.ac.uk)

F. W. Menk, School of Mathematical and Physical Sciences, University of Newcastle, Callaghan, NSW, 2304, Australia.